Reservoir imaging using low frequencies of seismic reflections

Gennady Goloshubin and Connie VanSchuyver, University of Houston, Texas, USA
Valeri Korneev, Lawrence Berkeley National Laboratory, California, USA
Dmitry Silin, University of California at Berkeley, USA
Vjacheslav Vingalov, West-Siberian Research Institute of Geology and Geophysics, Tyumen, Russia

There are numerous laboratory and field examples in which low-frequency components of reflected seismic waves show surprising imaging capabilities. Ironically, such components are often filtered out as useless in conventional data processing. However, as we demonstrate below, this part of the signal contains the most important information about the reservoir.

Let us consider three examples of field data processing. In all of them, the hydrocarbon-rich zones of the reservoir were localized using low-frequency analysis. These zones were confirmed on the basis of experience with well-production data. The imaging analysis was performed without well data. Note that conventional methods of data processing could not detect the hydrocarbon zones.

Example 1. This example demonstrates that oil-rich zones in natural reservoirs augment reflective properties at low frequencies. The data for this example were obtained from the Ai Pim oil field in the central region of Western Siberia. The log and core measurements in this field indicate the presence of two types of oil reservoirs. The first oil reservoir is at a depth of 2300 m (twt ~ 1.9 s) and consists of a productive layer (AC11), with thickness of 11-15 m, of coarse sandy Cretaceous siltstone. Below, there is the second oil reservoir (Ju0), which has a thickness of 15-20 m and consists of fractured bituminous Jurassic argillites. Conventional processing yielded the seismic time cross-section shown in Figure 1a. The seismic section has high resolution, which makes it possible to map the local small-amplitude structures and stratigraphic nonconformities. A comparison of the seismic cross-section and test results shows no correlation between the reflective properties of layers AC11 and Ju0 and the character of fluid saturation. Neither the amplitude nor the shape of the signal changes along the seismic horizon. Figure 1b shows the result of low-frequency processing with a wavelet transform of 12 Hz. The oil content of both strata (AC11 and Ju0) is depicted as an amplitude anomaly in the low-frequency compo-

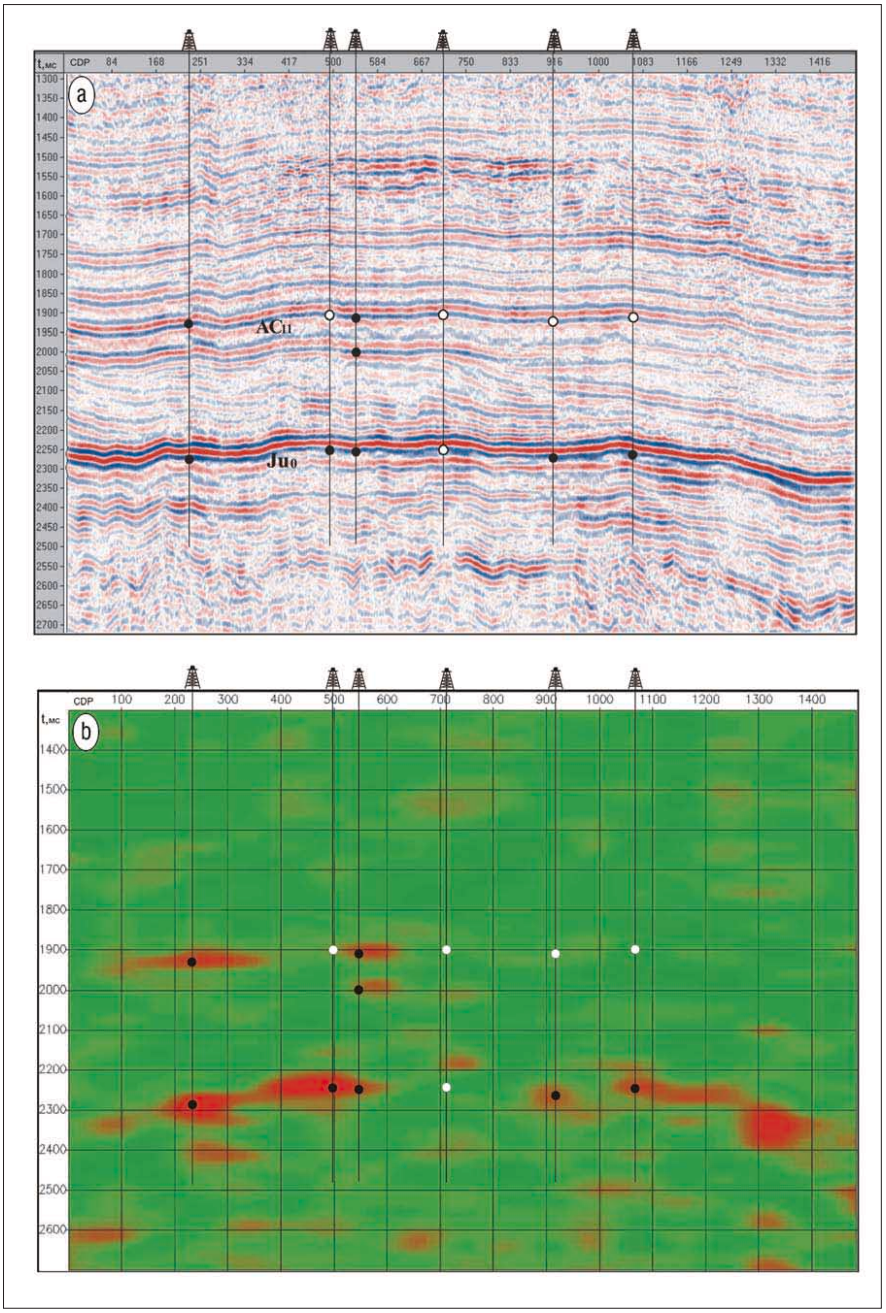

Figure 1. *A seismic line from Ai Pim Western Siberia oil field was used to image two different types of oil-saturated reservoirs. Black dots show where there is oil; white dots show where there is no oil. The well data indicate that the upper reservoir (marked AC11, the pore sandstone reservoir) consists of 11-15 m thick sandstone with varying fluid content. The lower reservoir (marked Ju0, the cracked shale reservoir) is represented by 15-20 m thick fractured shale. There is no evident correlation between well content and high-frequency standard seismic imaging (a). In contrast, the oil-saturated domains of the both AC11 and Ju0 create high-amplitude, low-frequency (<15 Hz) reflections (b).*

nent. It should be noted that the lithologic properties of strata AC11 and Ju0 are considerably different.

Figure 1a also shows the locations of the wells, whose production data were used for verification of the imaging. The black circles depict the intervals of successful oil production; the white circles mark the intervals where the produced fluid was mostly water. There is a strong correlation between the locations of the black circles and bright spots on the low-frequency image (Figure 1b); the locations of the white and black circles are not distinguishable from the point of view of conventional analysis (Figure 1a).

Example 2. Next, a 3-km-deep Jurassic sandstone reservoir is investigated (J1, Figure 2). The reservoir thickness is approximately 8–10 m with mean porosity of 17–18%. Seven of the 15 available wells produced oil, and six produced water, and two wells produced equal mixture of oil and water. Shown are four calibration wells, three of which (76, 91, 95) produced oil; the fourth one (9) produced water. In a blind test, the data from the other 11 wells were used only as a basis for verification of the mapping. Figure 2 shows a time map of the target horizon J1.

Figure 3 shows the results of frequency-dependent processing of this data set. The seismic imaging map shows the difference between the amplitude of the target reflected wave at low frequency (12 Hz) and the amplitude at high frequency (40 Hz). The imaging results *predicted* the location of oil-water contact. These results were confirmed by the well data. All wells producing water are outside of the oil-saturated region. The wells with the highest oil production rate (e.g., wells 91 and 86) are found close to the zones of great deviation in the map attribute.

Example 3. The third example is based on 3D seismic data from a field in South Marsh Island in the Gulf of Mexico. The reservoir is about 3 km deep and its sandstone layer is 8–10 m thick with a porosity about 0.35. The rock permeability is relatively high at 1–2 darcy. The low-frequency analysis was performed "blindly." The well locations were provided only after the seismic imaging of the reservoir zones. Even along the same line, the seismic sections of AVO attributes at different frequencies produce different images (Figure 4).

There is no visible anomaly displayed in the lower part of the section (Figure 4a) that represents conventional AVO attributes. In contrast, the low-frequency (10 Hz) AVO attribute section (4b) contains a bright anomaly around the reservoir depth (twt ~ 2.7 s).

Figure 5 shows an amplitude map of the low-frequency AVO attributes along the reservoir surface. The low-frequency AVO attribute map correlates well with the known production.

The fact that reflections from fluid-saturated solids are frequency-dependent has been discussed in the literature (Dutta and Ode, 1983; Denneman et al., 2002). Frequency-dependent processing and analysis of VSP data collected by monitoring gas/water-saturated dolomite layer (Goloshubin et al., 2001; Korneev et al., 2004) and instantaneous spectral analysis of seismic data (Castagna et al., 2003) clearly show that the low-frequency modes of the seismic wavefield are very informative during the study of fluid-saturated media.

Recently, Silin et al. (2004) have obtained an asymptotic representation of the seismic reflection from a fluid-saturated porous medium in the low-frequency domain. It turned out that the frequency-dependent component of the reflection coefficient is proportional to the square root of the product of frequency of the signal and the mobility of the fluid in

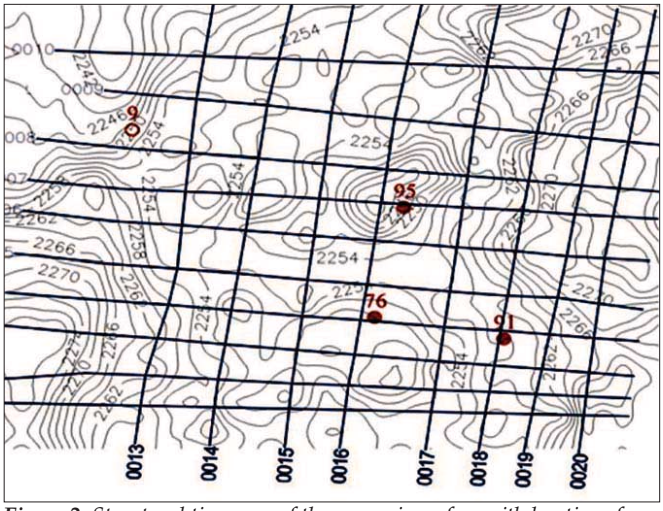

Figure 2. *Structural time map of the reservoir surface with location of four calibration wells, three of which (76, 91, 95) produce oil; the fourth (9) produces water. Note the poor correlation between medium structure and fluid.*

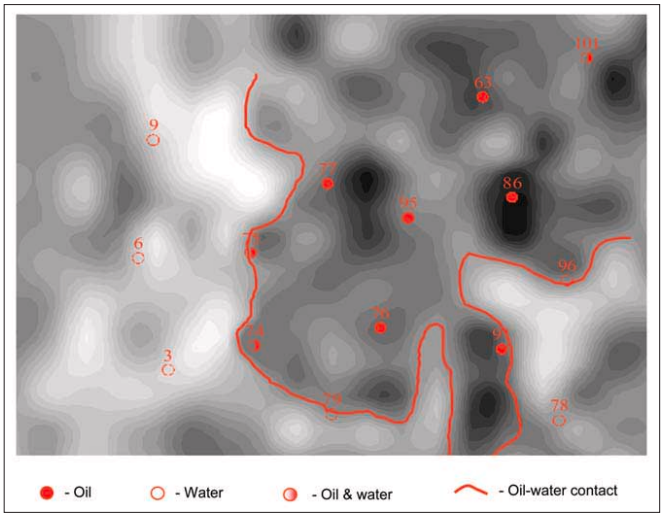

Figure 3. *A blind test of the ability of frequency-dependent processing and interpretation to map the oil-water contact using the low-frequency part of seismic data. The seismic and well data were recorded in central Siberia. The seismic image shows the difference between low-frequency reflectivity at 12 Hz and the one at 40-Hz centered frequency, the predicted oil-water contact (red line), and the locations of the calibration wells and the wells used for testing purposes.*

the reservoir. If we consider the reflection of frequency ω from the surface of a porous fluid-saturated reservoir, then the expression of the reflection coefficient R has the following form:

$$R = R_0 + R_1 (1 + i) (\omega\, k/\eta)^{1/2} \qquad (1)$$

Here R_0 and R_1 are real coefficients and i is the imaginary unit, k is reservoir permeability, and η is fluid viscosity. The coefficients R_0 and R_1 are dimensionless functions of the mechanical properties of the fluid and rock, which include the densities and the elastic coefficients. At $\omega\, k/\eta = 0$, the absolute value of the reflection coefficient attains its low-frequency maximum.

For the data in Figure 3, the imaging attribute $A(x,y)$ is proportional to the first derivative over the frequency of the reflected amplitude at a fixed (low) frequency. Taking into account equation 1, this implies the following relationship:

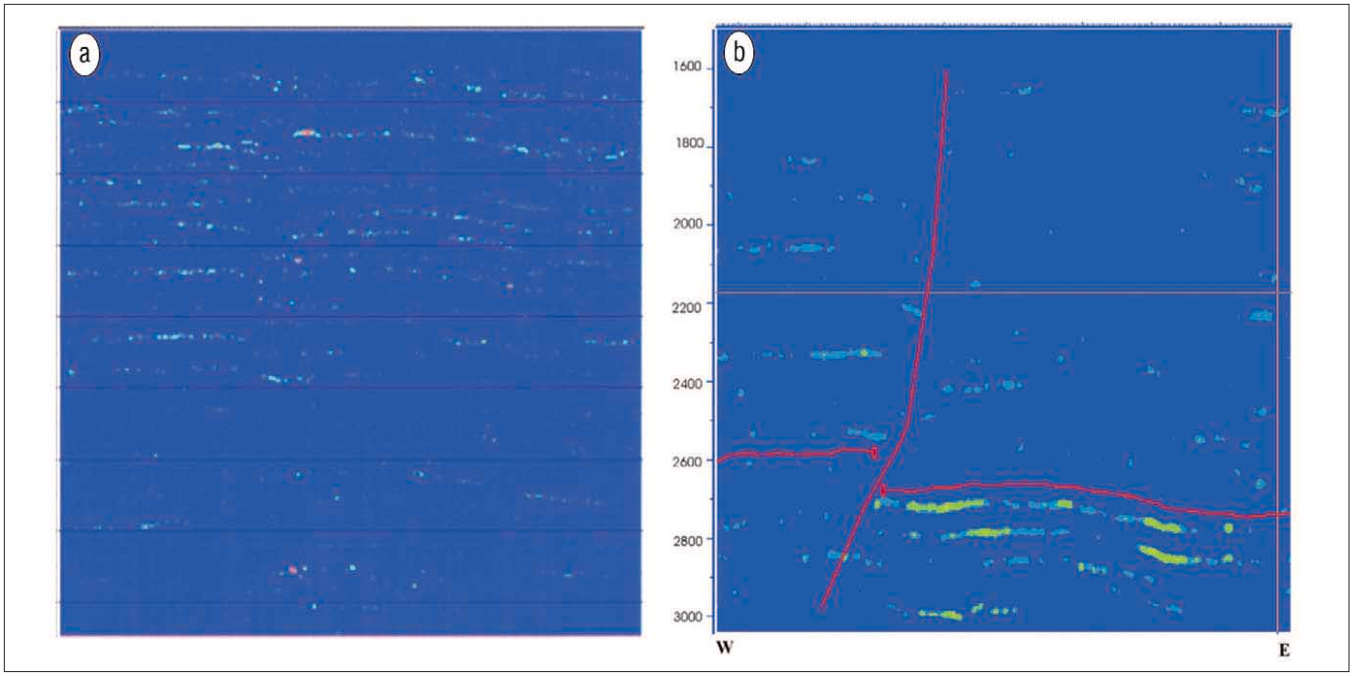

Figure 4. *The vertical seismic sections present the AVO attributes (intercept x gradient) at both high frequencies (a) and low frequencies (b). The low-frequency (10 Hz) AVO attributes section (b) contains a bright anomaly at the reservoir depth (twt ~ 2.7 s).*

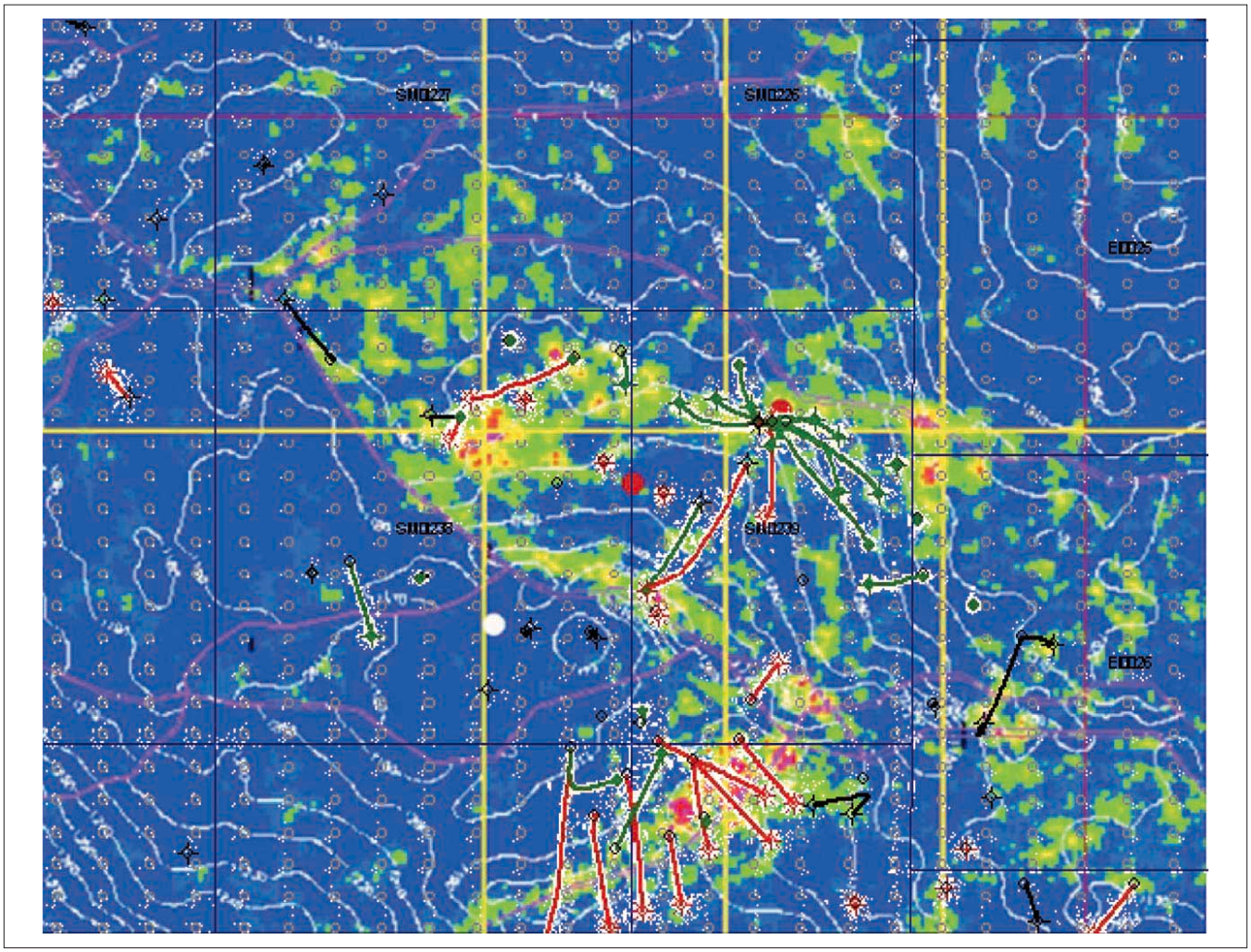

Figure 5. *Blind test result for the Gulf of Mexico data. The well data indicate that the oil and gas reservoir consists of an 8–10-m-thick sandstone at about 3 km deep with porosity about 0.35 and very high permeability (1–2 darcy). 3D seismic data were used for recognition of the reservoir zones and imaging of the oil-saturated areas. The plan view map includes the AVO attributes of low-frequency reflectivity at about 10 Hz along the surface of the reservoir. Well data show the reservoir saturation and production activity.*

$$A(x,y) \approx C\,(k/\eta)^{1/2} \qquad (2)$$

holds true, and the imaging attribute is therefore proportional to square root of fluid mobility. Using well data we can find the unknown constant C which is a complex function of porous rock parameters. Assuming that the well production rate is proportional to mobility, we can compute the theoretical curve for the production rate versus the imaging attribute. Figure 6 shows the measured production rates for the oil field from Figure 3, and the theoretical curve, which was calibrated using just one well data point. The field data and theory correlate quite well.

From the examples above it is clear that seismic reservoir imaging at low frequencies has great potential. Working from the assumption that robust amplitudes are obtained for individual frequency components of the propagating wavelet, we can calibrate seismic frequency-dependent reflectivity measurements to reservoir properties. However, the frequency content of the seismic wavelet is distorted by conventional data processing, with NMO providing the most significant distortion. In a conventional CMP gather, the trace associated with an offset equal to depth has a wavelet frequency that is nominally 12% lower than the wavelet frequency associated with the normal-incident reflection. Using anisotropic NMO processing, the wavelet frequency content on the very far-offset trace can be almost one-half that of the normal-incident wavelet—not an acceptable condition when calibrating loss mechanisms to reservoir properties as a function of frequency. In addition, AVO attributes are suspect when appreciable NMO stretch is generated. Hilterman and VanSchuyver (2003) introduced a novel processing and interpretation scheme based on a migration algorithm that doesn't perform NMO corrections followed by a target-oriented NMO correction. With target-oriented processing and interpretation, the reservoir time horizon is picked first, then the final NMO is applied to block-shift the offset traces within a CMP gather to the horizon time of the specified CMP gather. Because of the block shift, interpretation and data analyses are normally limited to a time window of about 100 ms on either side of the reservoir event.

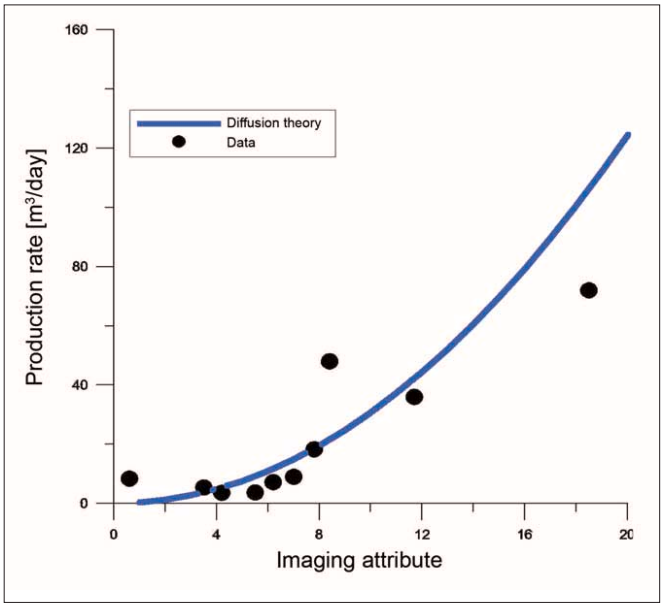

Figure 6. *The oil production rate versus the imaging attribute. The theoretical blue line is computed using the low-frequency asymptotic solution (equation 2).*

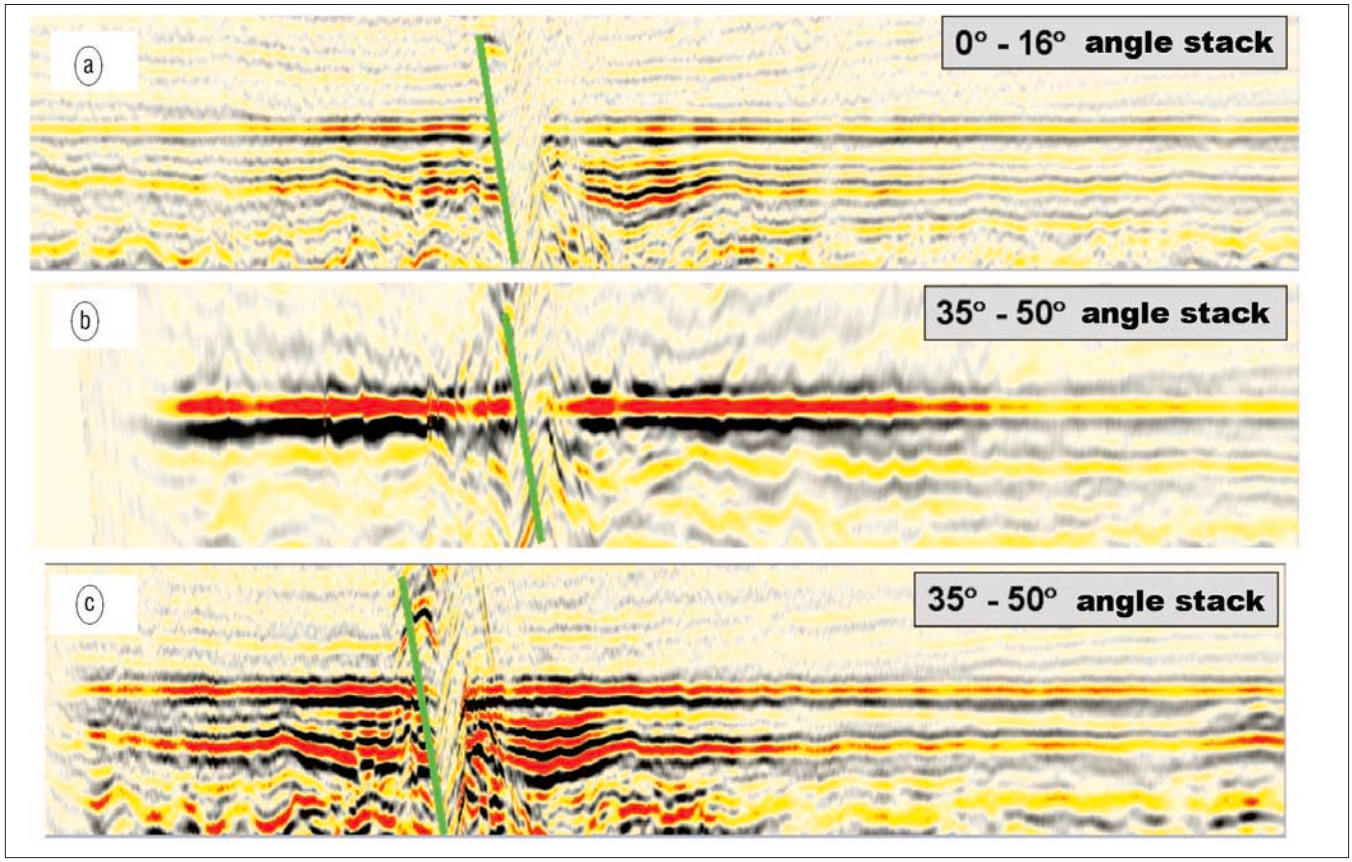

Figure 7. *(a) Conventional 0–16° angle stack. Data were flattened to top of structure. (b) Conventional 35–50° angle stack. (c) Target-oriented 35–50° angle stack. The CDP offset ranges in (b) and (c) sections contain incident angles beyond the critical angle.*

Besides the preservation of frequency, the quality of the seismic image is improved significantly with target-oriented processing. Figure 7 illustrates this point with an obvious improvement in both wavelet preservation and structural interpretation. To observe the frequency content of the signal, the upper surface of the high-amplitude reflection was flattened to a constant time. The fault location is illustrated with a green line on both the angle stacks. With conventional processing, the 35–50° angle stack in Figure 7b has excessive wavelet stretch and the interpretative value of the section becomes questionable. However, with target-oriented processing, the 35–50° angle stack in Figure 7c exhibits excellent quality. In fact, there are fault blocks illustrated on the 35–50° angle in Figure 7c that are difficult to observe in the 0–16° angle stack in Figure 7a. Once wavelet stretch is removed, we can expect this to result in better definition of faults on oblique reflection data.

Conclusions. Use of seismic low frequencies has a strong potential for prognoses of fluid content and mapping of productive highly permeable zones of the reservoirs. In the examples presented above, the low-frequency effects are especially important since no noticeable fluid signature was found in the high-frequency domain of seismic reflections from the oil-saturated reservoirs. Frequency-dependent seismic imaging allows the characterization of the subsurface fluid reservoirs in situations when other approaches fail. It is clear that NMO stretch needs to be avoided if quantitative analyses of amplitudes as a function of frequency are to be conducted. The target-oriented approach provides an avenue to avoid stretch. Still, several important problems must be addressed before the imaging technology is ready for routine use:

1) To date, the low-frequency imaging approach was applied to many different data sets. It turned out that it worked well in about 80% of the cases, while in other cases the interpretation outcome was uncertain. The limitations of the method need to be investigated so that the imaging procedure can be adapted to each situation (geology, data quality, frequency content, etc.).
2) Currently, no conventional seismic processing software has target-oriented processing. Numerous algorithms for interpretation need to be developed to handle this change in processing and interpretation philosophy.

Suggested reading. "Seismic reflections from a gas-water contact" by Dutta and Ode (GEOPHYSICS, 1983). "Reflection and transmission of waves at a fluid/porous medium interface" by Denneman et al. (GEOPHYSICS, 2002). "Seismic low-frequency effects in gas reservoir monitoring VSP data" by Goloshubin et al. (SEG 2001 *Expanded Abstracts*). "Instantaneous spectral analysis: Detection of low-frequency shadows associated with hydrocarbons" by Castagna et al. (*TLE*, 2003). "Seismic wide-angle processing to avoid NMO stretch" by Hilterman and VanSchuyver (SEG 2003 *Expanded Abstracts*). "Seismic low-frequency effects in monitoring of fluid-saturated reservoirs" by Korneev et al. (GEOPHYSICS, 2004). "A Hydrologic View on Biot's Theory of Poroelasticity" by Silin et al. (*Lawrence Berkeley National Laboratory Report 54459*, 2004). TLE

Acknowledgments: Seismic and well data were provided by Surgutneftegas and Fairfield Industries.

Corresponding author: ggoloshubin@uh.edu